Application of copper coatings onto used fuel canisters for the Canadian nuclear industry

Vo, Phuong; Poirier, Dominique; Legoux, Jean-Gabriell; Keech, Peter G.; Irissou, Eric

Publisher's version / Version de l'éditeur:

Applications of high pressure cold spray technology, 2015

Application of Copper Coatings onto Used Fuel Canisters for the Canadian Nuclear Industry

Phuong Vo, Dominique Poirier, Jean-Gabriel Legoux, Peter G. Keech*, and Eric Irissou

National Research Council Canada, 75 de Mortagne Blvd, Boucherville, QC, Canada
*Nuclear Waste Management Organization, 22 St. Clair Ave E, Toronto ON, Canada

1 Introduction

The Nuclear Waste Management Organization (NWMO) was established in 2002 under the Nuclear Fuel Waste Act (NFWA) to investigate approaches for managing Canada's used nuclear fuel. Currently, nuclear power plants are operating or undergoing decommissioning in Ontario, Quebec, and New Brunswick. Canada's CANDU reactors generate used fuel with small amounts of fissile nuclides compared to other types of nuclear reactors, owing to the use of unenriched uranium as a fuel source; used nuclear fuel is currently planned for disposal without reuse/reprocessing. The present approach, shown in Figure 1, envisions the conceptual long term storage of radioactive fuel bundles in specially designed canisters. The canisters would be emplaced in the rock of a suitable geological formation at a minimum of 500 m of depth, for an intended lifespan of more than 100,000 years (i.e., indefinite storage). The Canadian spent fuel canister consists of an inner container of steel strong enough to withstand geological pressures, including glaciations scenarios, and an outer shell of copper for corrosion resistance.

One reference container (1.2 m Ø × 4 m length) features a copper shell, which is up to 50 mm thick; this is predominantly a manufacturing necessity instead of performance requirement. For corrosion purposes, a much thinner layer of copper is required; a 100,000 year container life can

be achieved with less than 0.4 mm of copper. Under low salinity groundwater conditions, the corrosion allowance is 0.27 mm (fixed) for oxygen related corrosion and 0.1 nm/year for sulphide corrosion [1]. However, the use of conventional pierce/draw or extrusion methodologies to fabricate large copper shells from the extremely large copper ingots requires parts to retain significant strength to avoid collapse during manufacturing; this leads to large thickness dimensions. As a further manufacturing challenge, the requirement of a 1 mm nominal gap between the copper shell and inner steel container for assembly of the two piece container must also be met; this requirement is due to copper creep considerations. If the gap is too large, creep occurring under geological load can induce fracture of the copper; phosphorus doping helps to minimize creep-related fracture [2]. As an alternative, copper coatings directly deposited onto the steel canister offer the opportunity to produce a gap-free corrosion barrier, with no structural requirements. Copper cold spray is a promising methodology to provide sufficient corrosion protection to the steel canister while avoiding the handling and manufacturing issues associated with the wrought copper shell of the reference design described above.

Copper is one of the most common cold sprayed materials and an extensive knowledge base into myriad aspects is available in the literature. Indeed, early developmental work into cold spray technology by a number of researchers was performed using copper [3-8]. The effects of various spray parameters were recently reviewed by Assadi et al. [9] in their development of parameter selection maps for cold spraying, which show the relative influence, and relatively wide ranging possibilities, of gas temperature and gas pressure for copper cold spray. The characterization of microstructures and mechanical properties for copper coatings has shown that bulk-equivalent material can be obtained provided appropriate spray conditions and post-spray heat treatments

are employed [10-12]. Initial feasibility work for the specific application of cold spray copper on used fuel canisters has also been performed on small dimension samples by researchers at the Korea Atomic Energy Research Institute [13-15].

As part of a larger program investigating concepts of copper coatings, NWMO has recently begun exploring copper cold spray in collaboration with the National Research Council. Within the coating program, a large variety of copper coating sizes have been investigated, from small corrosion coupons to full scale used fuel containers (UFCs). Electrodeposition and various weld claddings are also coating technologies of interest; corrosion and mechanical performance programs are designed to support the use of copper coatings for UFCs. While it suffers from relatively small industrial usage when compared to the electrodeposition and cladding options, the versatility of cold spray coating has led to NWMO selecting it as a primary candidate for UFC coating; the extensive research and development (R&D) of the method are summarized below. While comprehensive to date, NWMO and NRC recognize that extensive validation work will be required prior to implementation of cold spray coatings for UFC manufacture.

2 Methodology

The preliminary development methodology consisted of four general stages: (i) powder selection, (ii) general coating development, (iii) used fuel canister coating optimization, and (iv) prototyping activities. Future activities will include an extensive validation study of the resultant methodology within a series of settings, including the R&D environment, pilot scale plant, and eventually a manufacturing plant, prior to the final selection of cold spray process inputs. During powder selection, a range of commercial powders were screened via powder and as-sprayed coating properties to determine two likely candidates. The two most promising powders were

then employed for general coating development to obtain an initial reference set of spray parameters and annealing conditions. In the third stage, reference parameters were optimized for UFC-specific materials and geometry. The prototyping stage involved final process adjustments and the production of mock-up assemblies in the R&D setting.

Photos of the various types of spray setups, with fixtures for smaller flat test substrates and larger spherical/cylindrical mock-up assemblies, employed in the various development stages are shown in Figure 2. The cold spray systems employed at various stages in the development process included the Kinetiks 4000 (Oerlikon Metco, Westbury, NY) and the PCS-800 and PCS-1000 (Plasma Giken Co., Ltd., Toshima-ku, Tokyo) using helium and/or nitrogen as the accelerating gas. Heat treatments were performed using a tube furnace with an argon atmosphere. A wide range of characterization methods were employed including, among others: powder size by laser diffraction; powder flowability by MPIF standard03; chemical analysis by inert gas fusion; particle velocity by time-of-flight optical particle diagnostics (cold spray meter); Vickers microhardness; surface roughness by stylus profilometer; surface topography by confocal microscopy; porosity measurement by image analysis; bond strength by ASTM C 633 [16] and/or modified ASTM E 8; tensile testing by ASTM E 8 [17]; bend testing by ASTM E 290 [18]; and microstructural analysis by Scanning Electron Microscopy (SEM) and/or optical microscopy.

3 Powder Selection

3.1 Initial screening via powder properties

For initial screening, 8 commercially available copper powders were selected and acquired from 5 different suppliers. Powders will be referred to hereafter by powder size (d_{50} value) and/or supplier (suppliers 1-5), where appropriate. Initial screening of the powders was performed through a characterization of the powder composition as well as powder size, morphology, and flowability. In general, the ideal powder size distribution (PSD) features average and maximum sizes as small as reasonably possible, due to the mass dependence of particle speed, and a minimum size greater than 8 μm, which is the critical particle diameter required for adiabatic shear instability with copper particles [19]. Unimodal particle size distributions are also favored as they tend to produce more homogeneous coatings. The flowability, which can be affected by powder size and morphology, is a practical consideration in powder feeding.

Table 1 compares chemical composition of the various feedstock powders with C10100 specifications. The C10100 reference was initially established by NWMO as it is one material that is extensively used in corrosion testing for its high purity of copper (> 99.99 %). A second reference copper within NWMO and other nuclear waste organizational work is oxygen free phosphorus doped copper (CuOFP), a form of copper with similar corrosion properties in deep geological repositories, but with improved creep ductility properties owing to the 30-100 ppm phosphorus doping [20]. All feedstock powders exceeded the allowable P level for C10100; this was not deemed to be detrimental to the subsequent corrosion test program. Most powders also exceeded C10100 limits for Sn, Fe, and Zn while excess Ag, Bi, Mn, Ni, Pb, Sb and Se were found in some; this may indicate a need for emphasizing powder procurement or manufacturing

in future NWMO programs, should highly pure coatings be desirable. Overall, supplier 1 powders displayed the highest purity and the analysis suggests that C10100 specifications could be met, if required, with the proper manufacturing method and raw material composition.

Among the examined powders, spherical powders were produced using gas or plasma atomization while the irregular powder was produced using water atomization. Powders from suppliers 4 and 5 displayed relatively high oxygen content with values of 1.130 % and 0.211 %, respectively. The latter value was somewhat surprisingly high as the plasma atomization manufacturing process was performed in vacuum; although it possibly can be explained if it was from an old powder lot. The oxygen content varied from 0.022 % to 0.113 % for other powders, with higher values for the smaller powders due to their higher specific surface. Feedstock powders were kept in a glove box under an inert, nitrogen atmosphere between spraying sessions to prevent oxidation. Should it be determined that the final application requires ultralow oxygen level coatings, emphasis must be placed on the proper handling of the feedstock powders as this can result in a higher gain in oxygen content than the cold spraying process itself.

A summary of powder size and flowability is also shown in Table 1. Powder d_{50} values ranged from 20 μm to 49 μm, with suppliers 1, 2, and 3 each providing two size distributions. Larger average particle size powders from the same supplier displayed a better flowability value than their smaller counterparts. In addition to the differences in size distribution, the surface appearance and morphology of powder particles from suppliers 1, 2, and 3, shown in Figure 3, can also be broadly described, respectively, as the following: spherical and satellite free (a-b); irregular and satellite free (c-d); and spherical with fine satellites (e-f).

Initial screening via powder properties eliminated powders from suppliers 4 and 5 due to very high oxygen contents (> 0.2 %) and/or poor flowability (e.g., leading to a failed test for supplier 4 powder). However, irrespective of deviations from the C10100 specification, the remaining six candidates were deemed acceptable in composition, size, and flowability. Consequently, powder selection between these six powders was performed via characterization of coating properties.

3.2 Powder selection via coating properties

The six candidate powders from suppliers 1-3 were N_2-sprayed using three gas temperature/pressure combinations (400 °C/2 MPa, 600 °C/3 MPa, and 800 °C/4 MPa), with other spray conditions summarized in Table 2. Coatings of 0.3-1.0 mm thickness were produced on 3.2 mm thick plates and > 50 mm thick cylinders of low C steel, with the latter used for bond strength testing. The powder particle velocities were measured and coatings screened by bond strength, porosity, and microstructure.

The highest particle velocities were obtained with the irregular powder from supplier 2, due to the higher drag force in that case. However, particle velocities of all powders measured at these conditions, ranging from ~ 480 m/s to 820 m/s, appeared to be within the deposition window between the erosion and critical velocities needed to provide high-quality coatings with good deposition efficiencies (~ 400-1100 m/s) [21]. Here, the critical and erosion velocity lines correspond to the simulated values for 25 μm cold particles; although both velocities depend on the particle size, temperature, oxygen content, and substrate surface temperature.

The ASTM C 633 bond strength values were as high as 41 ± 5 MPa for 350 μm to 630 μm thick coatings. While higher particle velocity somewhat favored coating adhesion, the relationship between specific powders, spray conditions, and bond strength was inconclusive. All powders allowed for the production of relatively dense coatings at the highest gas condition (800 °C/4 MPa). Some porosity was observed at lower (temperature/pressure) gas conditions and porosity measurements of coatings produced at 600 °C/3 MPa indicated that particle velocities above ~ 600-650 m/s resulted in less than ~ 0.5 % porosity. Smaller powders (and associated higher velocity) typically yielded lower porosity coatings than larger powders, although both d_{50} = 26 μm and d_{50} = 49 μm powders from supplier 3 displayed relatively high porosity coatings. This was assumed to be due to low associated particle velocities, although the fine surface satellites may also play a role.

Based on the above coating characterization, no single powder proved to be significantly better than other powders. However, additional testing with the d_{50} = 26 μm powder from supplier 3 revealed clogging of the powder injector and as a result, supplier 3 powders were eliminated. As is very often the case, no specific powder characteristics were identified as the cause of clogging of this powder over the others. Clogging is a general issue that limits the number of powders available for practical use in cold spray. The powder/nozzle material couple as well as nozzle and powder injector design are important aspects to consider for nozzle clogging. Spraying parameters, such as a high process gas temperature, can also trigger nozzle or injector clogging; although this was minimized with the use of the PCS-1000 gun that integrates nozzle cooling. It is also worth noting that clogging will be increased at higher feed rates, such as the very high rates that will be eventually targeted for production, because the charge effect will change the

structure of the gas flow. In general, powders in the coarser range are recommended as they offer better flowability, which is an important aspect in cold spraying. However, dense coatings were produced from most powders studied regardless of their different attributes, which suggests easy powder supply and availability from multiple sources.

4 General Coating Development

A comprehensive program was performed to investigate the effects of spray conditions and post-spray heat treatment conditions on copper coatings produced using a typical cold spray setup (i.e., an XY spray pattern on a generic substrate). The objective of this stage was to develop a set of reference process parameters that would be optimized in subsequent UFC coating development and prototyping stages (described later). For the sake of brevity, only selected results will be discussed in this section. Extensive literature is available concerning the general and fundamental aspects of cold spraying copper coatings [3-12].

4.1 Selection of coating parameters

For the selection of general copper coating spray parameters, an 18 run DOE was performed varying powder, gas type, gas temperature, gas pressure, gun traverse speed, step size, and/or standoff distance. The values employed for each parameter are shown in Table 2. The d_{50} = 42 μm and d_{50} = 23 μm powders from suppliers 1 and 2, respectively, (c.f., Figure 3a and c, respectively) were employed with the former powder displaying relatively low oxygen content, high flowability, and high coating bond strength while the latter powder offered an alternative (irregular) morphology and smaller size distribution. Coatings were produced on low C steel puck substrates (25.4 mm Ø × 6.35 mm thick), shown in Figure 2a, that were grit blasted with grit 24 (~ 975 μm) alumina.

A chemical analysis of selected coatings showed oxidation due to the cold spray process was limited. Coatings sprayed at 800 °C with N_2 gas using d_{50} = 42 μm, displayed 0.066 % compared to as-received powder values of 0.054 %. The similarity of oxygen content in powders and coatings was also observed during testing for the powder selection (not shown). Switching to He gas spray at 350 °C in an enclosed He atmosphere did not significantly change the oxygen pickup with 0.018 % measured for a coating with d_{50} = 42 μm powder.

The ASTM C 633 bond strength of coatings sprayed onto the 6.35 mm thick steel pucks ranged up to 29.4 ± 9.9 MPa, although the majority of coatings displayed bond strength values below 10 MPa. Aside from the He-sprayed coating, bond strengths greater than or equal to ~ 20 MPa were only obtained using gas temperatures of 800 °C. The variation in bond strength obtained for coatings produced during the DOE runs as well as the powder selection tests illustrate the difficulty in developing optimal spray parameters for coating adhesion; in principle, bond strength is a very important coating parameter for the program of producing UFCs. Bond strength may be influenced by specimen preparation, coating parameters, substrate condition, residual stresses, etc.

Overall, the capability of cold spray to produce fully dense copper coatings using a wide range of spray parameters was demonstrated by the DOE runs (measured porosity was less than or equal to 0.4 ± 0.6 % for all coatings). For a relatively low strength, ductile metal such as copper, the window of deposition of ~ 400-1100 m/s [21] is well within the capability of cold spray equipment. The average particle velocity measured for 13 different spraying conditions (powder with d_{50} =

42 μm) ranged from 570 m/s to 750 m/s, as shown in Figure 4, with optimized conditions at the upper end of the measured range. In comparison, average particle velocities measured for the various powders during the powder selection stage ranged from 480 m/s to 820 m/s. The effects of the spray parameters are typically linked to impact particle velocity, particle temperature, and substrate temperature due to their influence on the particle deformation. Coatings with greater degrees of particle deformation are typically associated with minimal porosity, high amounts of bonded area, and relatively high values of cohesive strength [9].

4.2 Selection of annealing conditions

For initial investigation of post-spray annealing, 3 mm thick coatings were produced on low C steel plate substrates (165 mm × 140 mm × 3 mm), shown in Figure 2b, using He-spray and N_2-spray . For brevity, only results with N_2-sprayed, d_{50} = 23 μm-powder coatings will be presented in this section. A range of annealing conditions based on the temperatures of stress relieving and annealing of pure wrought copper was screened through microhardness and microstructure characterization. Annealing temperatures of 200 °C, 300 °C, 400 °C, 500 °C, and 600 °C for 1 h and 10 h were investigated as well as one long term – low temperature anneal at 200 °C for 100 h. Two optimized conditions were then selected for subsequent characterization by ASTM E 8 tensile testing, ASTM C 633 bond testing, and ASTM E 290 bend testing. Coatings were machined to eliminate surface irregularities for bend and bond testing (0.8-1.1 mm removed) and to produce 1 mm thick coating-only specimens for tensile testing.

Based on the hardness measurements and microstructure analysis of the micrograph coupons in screening tests, the following two optimized annealing conditions were identified: 1 h at 300 °C

and 1 h at 600 °C. The first condition featured a relatively low temperature that produced a significant decrease in hardness from the as-sprayed condition as well as no apparent increase in porosity, as shown in Figure 5a and Figure 6b, respectively. The second condition employed a relatively high temperature that produced microstructural restoration (i.e. recrystallization) in the annealed coating (Figure 6c). The 1 h anneal time was selected due to the minimal hardness difference obtained between 1 and 10 h.

Bond strength was high for coatings in both as-sprayed and annealed conditions. Samples generally failed in the epoxy (used to attach the pull test studs in ASTM C 633), which indicated bond strength was at minimum equal to the epoxy strength of 60-70 MPa. Representative stress-strain curves for coatings in the as-sprayed and annealed conditions, shown in Figure 5b, revealed that annealing decreased coating strength and increased ductility, with a greater effect obtained at higher temperature. Tensile strength and strain at failure values of 370 ± 33 MPa and 0.5 ± 0.2 %, 245 ± 4 MPa and 16 ± 3 %, and 180 ± 2 MPa and 34 ± 3 % were obtained for as-sprayed, 300 °C annealed, and 600 °C annealed conditions, respectively. These results are consistent with reported values in the literature for cold spray copper coatings [10, 11]. For comparison, the ASTM B 152 [22] minimum tensile strength is 205 MPa for hot-rolled tempers and 220-360 MPa for cold-rolled tempers with a minimum 40% elongation for C11000 and C12200 plate with hot-rolled tempers; it is worth noting that such a large minimum requirement is unlikely to be utilized for UFCs. Typical bend test specimens, shown in Figure 5c, produced a crack through the entire coating within a 5 ± 1 ° bend for the as-sprayed condition; a first edge crack after a 52 ± 14 ° bend and 90 ° bend without a crack propagating through the entire

coating thickness after heat treatment at 300 °C; and no visible cracks after a full bend (146 °) in samples annealed at 600 °C.

The coatings in as-sprayed condition displayed a relatively smooth fracture surface and clearly delineated particle boundaries (Figure 6d). In contrast, a dimpled fracture surface without discernable particle boundaries was observed in coatings annealed at 600 °C (Figure 6f). From these results, it may be interpreted that fracture was associated with particle de-bonding (e.g., the as-sprayed condition) and the improvement in ductility after annealing was potentially due to better inter-particle bonding (e.g., the 600 °C heat treatment) [10, 11]. Heat treatment at 300 °C represented a transition between these conditions (Figure 6e), so only moderate ductility improvements were observed.

In this work, the effect of the increase in porosity observed in coatings annealed at 600°C (c.f., Figure 6c) was not evaluated. Calla et al. [10] also obtained an increase in apparent porosity located at inter-particle boundaries in cold sprayed coatings annealed at 600°C for 1 h. This increase was cited as a potential source of the lower ductility obtained for annealed coatings relative to annealed bulk sheet, and attributed to a possible relaxation of compressive residual stresses or the expansion and spheroidization of driving gas entrapped within the cold spray structure. Stoltenhoff et al. [12] observed the development of spheroidized oxides in coatings annealed at 600°C for 1 h, which were located at former inter-particle boundaries in N_2-sprayed coatings and randomly distributed in He-sprayed coatings. Another potential cause of the increase in observed porosity is the spheroidization of pores through a mechanism analogous to sintering, which has been reported for other cold sprayed material [23]. In that case, the increase in apparent porosity

would result from a reorganisation of the initial planar defects (inter-particle boundaries) into spherical and thus more visible pores, and not from an actual/real increase in porosity. In general, the effects of porosity are dependent on the amount, size, and morphology of the pores. Pores can act as defects which raise stress concentrations and although no porosity – strength relationships are available for cold sprayed copper, Hyun et al. [24] showed tensile strengths of ~ 150 MPa can still be obtained with as much as 2-3 % porosity for copper castings. To date, no specification on allowable porosity has been defined for the UFC application.

5 Used Fuel Container Coating Optimization

Based on the general coating development above, parallel coating feasibility studies (not shown), and UFC container requirements, an initial reference cold-spray coating system was defined. In order to maximize coating adhesion, a bond coat sprayed with He was selected, followed by a N_2-sprayed top coat to build the required thickness. However, such a process was not sufficiently validated to implement on mock-up containers. In addition, post deposition heat treatment was only roughly defined at this point in the study; results from parallel modeling in-repository container performance, conducted concurrent with cold spray feasibility studies, were able to better define copper coating ductility requirements. Finally, only planar coupons of various steel grades were cold-spray coated within the feasibility studies indicated above. To be considered for UFCs, it was necessary to demonstrate that cold spray coating can be achieved on materials such as: steel grade of the UFC body, welded steel substrates, larger dimension steel coupons, and cast iron substrates, prior to implementing a program dedicated to UFC fabrication.

5.1 Validation of reference coating on planar substrates

The initial reference cold-spray coating system was defined with the following parameters:

- 10-70 μm spherical low oxygen copper powder;
- 25.4 mm min. thick A516 grade 70 steel, grit blasted with 24 grit to remove mill scale;
- 100 μm bond coat, applied with He-spray at 5 MPa and 800 °C; and
- 3 mm top coat, applied with N_2-spray at 5 MPa and 800 °C.

Based on powder availability and reference powder criteria, the d_{50} = 42 μm powder from supplier 1 used previously for general coating development was selected for validation testing and two new powder lots were obtained. To maintain continuity and avoid confusion, the powder will be generically referred to as d_{50} = 42 μm powder (with lots A, B, or C, when applicable). The original lot (A) and two new lots (B and C) were similar in size distribution (d_{50} = 42 μm, 48 μm, and 43 μm, respectively) and all three lots displayed a dense, spherical morphology with particle surfaces free of satellites.

Initial validation trials were performed using the Plasma Giken PCS-1000 unit and powder lot B and involved coatings produced on the flat surface of cylinders (25.4 mm Ø × 38.1 mm) held in a rotating substrate holder (15 cm Ø), shown in Figure 2c. The A36 steel substrates, which are compositionally similar to the reference A516 grade 70, did not significantly affect the coating density or bond strength (detailed later). The first spray trial using initial reference parameters produced a visually uniform coating surface and ASTM C 633 bond strength testing resulted in epoxy failure (i.e., min. 60-70 MPa). The coating microstructure, shown in Figure 7a, displayed a dense ~ 340 μm thick bond coat produced by He-spray and an additional ~ 3 mm was subsequently deposited by N_2-spray with coating porosity measured at 0.1 ± 0.1%.

An attempt to spray with powder lot C using initial reference conditions showed clogging issues, which were not obtained with A or B powder lots. A difference in oxygen content for lot C and/or a higher amount of fines may have been significant. A change in gas temperature (from 800 °C to 600 °C) and spray unit (from PCS-1000 to PCS-800) from the initial reference was employed to resolve the clogging. Coatings produced using the lower gas temperature, as well as increased substrate rotation speed in view of accommodating the practical aspects of spraying the large diameter UFC detailed later in prototyping, were dense (0.1 ± 0.2 % in ~ 3 mm top coat) and achieved comparable bond strength minima to the previous materials. As the lower temperature parameters were necessary to avoid clogging with one of the two powder lots used, the reference coating condition was modified to allow for a gas temperature of 600 °C for this lot.

A secondary validation through four production runs using larger scale substrates was performed using the Plasma Giken PCS-800 unit and powder lot C. Each production run involved depositing 3 mm thick coatings on plate substrates (A516 grade 70, 150 mm x 150 mm x 38 mm) fixed into a rotating 560 mm Ø sample holder, which also allowed puck substrates (25.4 mm Ø x 38.1 mm) to be simultaneously coated, as shown in Figure 2d. In addition to standard 3 mm thick coatings, 5 mm and 10 mm thick coatings were also produced. Two plates with 3 mm thick coatings were arbitrarily selected as representative coatings for characterization. During one production run, A36 pucks were simultaneously coated to produce specimens for immediate analysis (i.e., avoid machining delay) and confirm that spraying on A36 or A516 Grade 70, which have similar compositions, would not change coating properties. This latter equivalency

demonstration is particularly important in that the nearest steel to A516 Grade 70 plate in a rod form is A36. Coating porosity was measured at 0.5 ± 0.4 % and 0.3 ± 0.2 % for the plate and puck samples, respectively, from the same run, shown in Figure 7a-b. The other coated plate specimen appeared completely dense with porosity measured at 0.0 + 0.1 %. The coating-substrate interfaces were also similar and all bond strength tests resulted in epoxy failure (i.e., min. 60-70 MPa) instead of the coating-substrate interface. Due to the similarity in coating density, coating interface, and bond strength results, the effect of different substrates (A516 and A36) was considered minimal.

Bond strength measurement using a modified ASTM E 8 tensile test on small scale specimens (5.90 mm gage length × 20 mm^2 area cross section) was performed by an external contractor (Exova, Cambridge, ON) on the 10 mm thick cold spray coating on A516 plate. All failures were reported to occur at the coating-substrate interface with no measurable elongation and a bond strength of 83 ± 15 MPa. The bond strength was consistent with the ASTM C 633 results, which showed epoxy failures at > 60 MPa for 3 mm thick coatings on A516 plate. As coating adhesion decreases with increasing coating thickness, the minimum bond strength of the 3 mm thick coatings can be considered, at minimum, equal to the 10 mm thick coating (i.e., minimum 83 ± 15 MPa instead of minimum 60 MPa).

5.2 Application of reference coating to weld samples

The application of reference coatings on the weld area of A516 grade 70 substrates involved the same setup as the validation using A36 cylinders (c.f., Figure 2c-d). A cross-section of the as-received welded steel substrate (not shown) confirmed that the weld surface was much larger (~

35 mm wide) than the 25.4 mm diameter rod specimens machined from the weld area. Overall, the coatings produced on weld substrates under the conditions investigated were comparable in bond strength and coating density to the coatings produced during the reference parameter validation (e.g., epoxy failure in ASTM C 633 bond strength test and < 0.3 % porosity at T_g = 600 °C, shown in Figure 7c, using a He-sprayed bond coat with N_2-sprayed top coat).

5.3 Application of reference coating to cast iron substrates

The application of reference coatings on cast iron substrates were produced with the same procedure as the weld substrate samples. In general, coatings on cast iron displayed low porosity (0.4 ± 0.5%), shown in Figure 7d, which was similar to the reference A516 grade 70 (or A36) steel grade(s). However, bond testing produced adhesive failure at the coating-substrate interface with a measured strength of 37 ± 12 MPa, which was significantly below the epoxy failures at ~ 60-70 MPa for A516 (or A36) reference substrates. The relatively large standard deviation was due to one outlier at 14 MPa failure (i.e., 41 ± 3 MPa for other 4 replicates).

The root cause of the lower bond strength on the cast iron substrate was not clear, although differences were observed with coatings on reference substrates. The higher magnification SEM micrographs (250 ×) in Figure 7 reveal that the coating-substrate interface was generally more uniform (i.e., flat) on the cast iron substrate. Coatings on the A36 substrate qualitatively displayed more closely spaced peaks along the interface and a higher peak-to-trough distance, which suggest that deformation of the particle and/or substrate was higher than for the coating on cast iron. A lower degree of deformation may result in lower bond strength (e.g. due to a decrease in mechanical interlocking and/or adiabatic shear instability). Spheroidal (nodular)

graphite was distributed throughout the matrix (Figure 7d) with partial nodules observed along machined edges (not shown). However, these relatively large nodules were not observed along the coating-substrate interface, which suggests that nodules were removed during the substrate preparation (i.e., grit blasting) and/or spray process (i.e., particle impact). The presence of graphite at the interface (e.g. crushed fragments) may reduce bond strength by decreasing the well-bonded area between the copper particles and the matrix of the cast iron.

5.4 Optimization of annealing conditions

Results from the initial study for general coating development showed that coatings heat treated for 1 h at 300 °C did not quite meet the preliminary ductility requirement (20 % elongation prior to fracture) while coatings heat treated for 1 h at 600 °C displayed small pores not observed in the as-sprayed condition. As a result, a brief optimization of annealing conditions was performed. Planar samples coated with the reference coating system were tested in the as-sprayed condition and after heat treatment for 1 h at 350 °C and 400 °C.

The as-sprayed coating displayed a tensile strength of 171 ± 14 MPa and strain to failure of 0.2 ± 0.0 %. Heat treatment of coatings for 1 h at 350 °C and 400 °C produced increases in ductility values to 23.2 ± 3.0 % and 25.9 ± 6.6 %, respectively, as well as minor increases in tensile strength to 198 ± 7 MPa and 194 ± 11 MPa, respectively. Micrographs of the coating cross-sections indicated that coating porosity (as-polished, not shown) did not increase significantly after heat treatment at 350-400 °C, which was consistent with previous observations during general coating development. Instead, any differences in observed porosity were attributable to variations in the as-sprayed coating. Etched micrographs, shown in Figure 8, revealed the

development of equiaxed grains within deformed particles after heat treatment due presumably to recrystallization. Grain boundaries were not resolved in the as-sprayed microstructure (Figure 8a) and the deformed particle boundaries were heavily over-etched in order to reveal grain boundaries in the coatings annealed at 350 °C and 400 °C (Figure 8b and c, respectively). Overall, the mechanical and microstructural characterization demonstrated that coatings heat treated for 1 h at 350-400 °C displayed acceptable strength and ductility, although the 400 °C anneal may be more preferable due to the development of more (qualitatively) uniform, equiaxed grains.

6 Prototyping

6.1 Process adjustments

In order to scale up from 150 mm × 150 mm planar samples to mock-up assemblies of up to 2.15 m length, the validated coating parameters required several process adjustments. Changes for substrate handling/preparation (e.g., lift system, portable grit blast, etc.) and productivity (e.g., increased feed rate) were relatively straightforward to introduce. In comparison, significantly greater effort was needed for the development of a new procedure for reducing He gas consumption. Although performed to accommodate facility He gas storage capability, this modification is also a step forward in process cost optimization.

For the prototyping activities, coating of the first cylindrical pipe segment was performed with the conditions validated for the planar samples (Section 5.1) while all subsequent coatings were produced with the adjusted conditions described here (Section 6.1). The reference coating

process for both N_2 and He gas spray used the same nozzle, which featured a nozzle diameter designed to maximize N_2-spray productivity. Consequently, a smaller (throat and exit) diameters nozzle optimized for He-spray was employed in order to reduce flow rate (~ 65 % lower) while still maintaining similar particle velocity (measured with N_2 gas only). A switch to the smaller diameter nozzle (for bond + top coats), with all other conditions kept constant, to produce a 3 mm thick coating on A36 cylinders (25.4 mm Ø × 38.1 mm thick) resulted in a bond strength of 42 ± 5 MPa, which was lower than coatings produced with the larger diameter nozzle (i.e., min. 60-70 MPa).

Upon obtaining these results, this difference was attributed to a lower substrate temperature caused by less gas flow through the smaller diameter nozzle. To investigate this hypothesis, the substrate surface temperatures were measured using an infrared camera, for simulated (i.e., powder free) deposition runs. The small nozzle resulted in 15-20 °C lower substrate temperatures. Consequently, the substrate temperature was raised using two simulated runs (without powder) prior to actual deposition runs, and the resultant coatings met bond strength requirements with a value of 61 ± 3 MPa (epoxy failure). Concurrently, it was found that the preheating could be done using a radiant lamp, for a similar bond strength result (58 ± 2 MPa, epoxy failure). Subsequent to the nozzle switch, the powder feed rate was increased from 80 g/min to 250 g/min in order to increase productivity. The increase in powder load did not adversely affect the coating porosity as measured via image analysis (not shown). However, a decrease in adhesion occurred (43 ± 7 MPa); principally due to the higher deposition rate per pass, and not the powder feed rate itself. When the rotation speed of the samples was increased

to match the deposition rate per pass obtained at lower feed rate, the coating adhesion was recovered (56 ± 5 MPa).

Coatings for prototyping were applied using the PCS-800 cold spray unit with two large volumes of powder lots of d_{50} = 42 μm powder (lots D and E). However, it was immediately found that the coatings produced using lot E displayed lower adhesion than the others. It was initially unclear if the poorer performance of this lot is due to a different powder surface state and/or a higher proportion of coarse particles in this lot (d_{90} = 62-67 μm lots A-D and 72 μm for lot E). Both powder sieving and powder heat treatment under H_2 helped to recover adequate coating adhesion, but only powder sieving was actually performed prior to prototyping coating.

6.1 Cylindrical body

The reference coating was applied to a ~ 300 mm length on a pipe segment of A106 schedule C steel (508 mm x 406 mm x 38 mm) fixed on a turntable, shown in Figure 2e. The He-sprayed bond coat, N_2-sprayed top coat, and machined surface displayed macro coating appearances similar to those obtained in the planar validation. Although not specifically measured or recorded during production, the He-sprayed bond coat thickness was estimated to be ~100-150 μm based on the planar validation results while the N_2-sprayed top coat thickness was 3.85 ± 0.20 mm (as-deposited). SEM micrographs of the coating (not shown) in locations at the top, mid-length, and bottom of the coated pipe revealed the coating to be completely dense at all three locations.

6.2 Hemispherical head

Two methods were used to coat the hemispherical heads: via simultaneous rotation of the heads and manipulation of the cold spray gun; and via sequential masking of stationary heads with gun manipulation. Figure 9a illustrates some developmental patterns explored during the former approach, which occasionally led to incomplete or uneven coverage, while Figure 9b illustrates the coating with mask used in the latter method. A pull backed view of the latter method is also shown in Figure 2f. Full sized heads were made using both approaches.

Specimens from the coating on the actual hemispherical head were machined by EDM (Figure 9c) and results showed good coating uniformity, except near the sphere apex. Coating adhesion was estimated following ASTM C 633 standard guidelines, although it must be noted that a bias was introduced by the curved coating surface (probable change in stress distribution and difficult alignment of the pull studs with the tensile axis). Coating adhesions between 35 MPa and 55 MPa were achieved; the highest value being obtained at the apex of the sphere. Upon fabrication, one coated hemispherical head was CNC machined (Figure 9d).

6.3 Mock-up and lower assembly

The coating process for the used fuel canister was first demonstrated on one mock-up assembly consisting of the cylindrical body, hemispherical head, and weld transition. This assembly represented a full diameter lower section of the canister (i.e., full size hemispherical head and weld transition) with a truncated cylindrical body (560 mm Ø × 620 mm part length). An actual lower assembly (full part length of 2270 mm) was subsequently coated. The setup for coating the

truncated assembly and full sized lower assembly, shown in Figure 2g and h, respectively, employed a horizontal frame with motorized rollers to rotate the assemblies.

Due to the assembly sizes, the coatings were applied in sections over multiple work days. This practical issue required the development of restarting procedures to account for surface preparation and blending/joining of the coatings deposited on previous sections. In principle, previous sections may undergo slight surface oxidation, which must be removed prior to overspraying; there is also a necessary substrate temperature to achieve satisfactory coatings, as discussed in the nozzle selection discussion of Section 6.1. Accordingly, the spray pattern was modified to produce a taper at the edge of the each day's section in order to mitigate coating variation at the transition between sections. Prior to spraying, the overlapping copper region was grit blasted at the same time as the new section to cover. Post deposition microstructural observations of companion coupons did not show any coating variation in overlap regions. Figure 10 shows the full sized lower assembly after coating of two sections and the entire assembly. Similarly to the hemispherical head, both assemblies were machined following deposition to remove macroscopic surface roughness (i.e., as per Figure 9d).

7 Conclusions and Future Work

The successful application of the cold spray coating technology to full scale geometric representative Mark II UFC mock-up configurations (carbon steel cylinder/spherical heads and applicable weld substrates) was demonstrated through activities involving (i) powder selection, (ii) general coating development, (iii) used fuel canister coating optimization, and (iv) prototyping. Reference spraying and annealing conditions were established, and coating quality and properties were validated on different substrate geometries and compositions. Results also

indicated that powder manufacturing and robust handling procedures are key considerations for reliability and consistency of coating properties. A clear path to manufacturing copper coatings on UFCs via cold spray deposition was developed, including details on (i) process parameter scale-up adjustment, (ii) spray set up and pattern development, (iii) coating joining procedure, and (iv) coating machining. Ongoing development of the coating process is focused on the weld closure zone, where the process will need to be adapted in order to limit the rotation of filled used fuel containers. The establishment of a clear operating window sufficient for large scale manufacturing of the process is also still required, and will be investigated in ongoing work.

References

1. Kwong, G.M. (2011). Status of Corrosion Studies for Copper Used Fuel Containers Under Low Salinity Conditions, NWMO TR-2011-14. Report from Nuclear Waste Management Organization.
2. Sandström, R., and Wu, R. (2013). Influence of phosphorus on the creep ductility of copper. J. Nucl. Mater., **441** 1–3, 364-371.
3. Dykhuizen, R.C., Smith, M.F., Gilmore, D.L., Neiser, R.A., Jiang, X., and Sampath, S. (1999). Impact of high velocity cold spray particles. J. Therm. Spray Technol., **8** 4, 559-564.
4. Gilmore, D.L., Dykhuizen, R.C., Neiser, R.A., Roemer, T.J., and Smith, M.F. (1999). Particle velocity and deposition efficiency in the cold spray process. J. Therm. Spray Technol., **8** 4, 576-582.
5. Van-Steenkiste, T.H., Smith, J.R., Teets, R.E., Moleski, J.J., Gorkiewicz, D.W., Tison, R.P., Marantz, D.R., Kowalsky, K.A., Riggs, W.L., Zajchowski, P.H., Pilsner, B., McCune, R.C., and Barnett, K.J. (1999). Kinetic spray coatings. Surf. Coat. Technol., **111** 1, 62-71.
6. Alkhimov, A.P., Klinkov, S.V., and Kosarev, V.F. (2000). Experimental study of deformation and attachment of microparticles to an obstacle upon high-rate impact. J. Appl. Mech. Tech. Phys., **41** 2, 245-250.
7. McCune, R.C., Donlon, W.T., Popoola, O.O., and Cartwright, E.L. (2000). Characterization of copper layers produced by cold gas-dynamic spraying. J. Therm. Spray Technol., **9** 1, 73-82.
8. Papyrin, A. (2001). Cold spray technology. Adv. Mater. Processes, **159** 9, 49-51.
9. Assadi, H., Schmidt, T., Richter, H., Kliemann, J.O., Binder, K., Gärtner, F., Klassen, T., and Kreye, H. (2011). On parameter selection in cold spraying. J. Therm. Spray Technol., **20** 6, 1161-1176.

10. Calla, E., McCartney, D.G., and Shipway, P.H. (2006). Effect of Deposition Conditions on the Properties and Annealing Behavior of Cold-Sprayed Copper. J. Therm. Spray Technol., **15** 2, 255-262(258).
11. Gartner, F., Stoltenhoff, T., Voyer, J., Kreye, H., Riekehr, S., and Kocak, M. (2006). Mechanical properties of cold-sprayed and thermally sprayed copper coatings. Surf. Coat. Technol., **200** 24, 6770-6782.
12. Stoltenhoff, T., Borchers, C., Gartner, F., and Kreye, H. (2006). Microstructures and key properties of cold-sprayed and thermally sprayed copper coatings. Surf. Coat. Technol., **200** 16-17, 4947-4960.
13. Choi, H.-J., Lee, M., and Lee, J.Y. (2010). Application of a cold spray technique to the fabrication of a copper canister for the geological disposal of CANDU spent fuels. Nucl. Eng. Des., **240** 10, 2714-2720.
14. Kim, S.K., Lee, M.S., Choi, H.J., Choi, J.W., and Kwak, T.-W. (2009). Progress of a cost optimization for an HLW repository in Korea. Prog. Nucl. Energy, **51** 3, 401-408.
15. Lee, M.S., Choi, H.J., Choi, J.W., and Kim, H.J. (2011). Application of cold spray coating technique to an underground disposal copper canister and its corrosion properties. Nucl. Eng. Technol., **43** 6, 557-566.
16. ASTM C 633 Standard Test Method for Adhesion or Cohesion Strength of Thermal Spray Coatings. (2001). ASTM International, West Conshohocken, USA.
17. ASTM E 8/E 8M - 09 Standard Test Methods for Tension Testing of Metallic Materials. (2009). ASTM International, West Conshohocken, USA.
18. ASTM E 290 - 09 Standard Test Methods for Bend Testing of Material for Ductility. (2009). ASTM International, West Conshohocken, USA.
19. Schmidt, T., Gartner, F., Assadi, H., and Kreye, H. (2006). Development of a generalized parameter window for cold spray deposition. Acta Mater., **54** 3, 729-742.
20. Sandström, R., and Andersson, H.C.M. (2008). The effect of phosphorus on creep in copper. J. Nucl. Mater., **372** 1, 66-75.
21. Schmidt, T., Assadi, H., GÃ¤rtner, F., Richter, H., Stoltenhoff, T., Kreye, H., and Klassen, T. (2009). From particle acceleration to impact and bonding in cold spraying. J. Therm. Spray Technol., **18** 5-6, 794-808.
22. ASTM B 152/B 152M - 06a Standard Specification for Copper Sheet, Strip, Plate, and Rolled Bar. (2006). ASTM International, West Conshohocken, USA.
23. Wong, W., Irissou, E., Legoux, J., Bernier, F., Vo, P., Yue, S., Sone, M., and Fukanuma, H. (2012). *In* "Cold Spray Forming Inconel 718" (Lima, R.S., Agarwal, A., M., H.M., Lau, Y.-C., Li, C.J., McDonald, A., and Toma, F.-L., (Eds.), pp. 243-248. ASM International (Materials Park, OH).
24. Hyun, S.K., Murakami, K., and Nakajima, H. (2001). Anisotropic mechanical properties of porous copper fabricated by unidirectional solidification. Mater. Sci. Eng. A, **299** 1–2, 241-248.

List of figures and tables

Figure 9 – Photos showing coating development for hemispherical head: (a) coated dishes (with matching geometry to the apex) used in the optimization of a curved spray pattern, (b) apex coated using an XY pattern with masking, (c) coated hemisphere sectioned for characterization, and (d) CNC machining of a coated hemisphere.

Figure 10 – Full sized lower assembly after coating of (a) two sections and (b) entire assembly.

Table 1 – Selected characterization data for feedstock powders.

Supplier, d_{50}	Chemical Analysis							PSD			Flowability
	Cu	O	Ag	S	Fe	Ni	Other [b]	d_{10}	d_{50}	d_{90}	
	%	%	ppm	ppm	ppm	ppm	ppm	µm	µm	µm	s/50 g
1, 20 µm	99.89	0.080	18	12	28	5	5P, 5Sn, 29Zn	9	20	34	5.2 [c]
1, 42 µm	99.92	0.054	27	11	3	7	4P, 2.2Sn	17	42	62	10.7
2, 23 µm	99.85	0.107	21	11	3	2	212P	14	23	35	22.4
2, 29 µm	99.83	0.113	11	12	71	11	198P, 92Sn, 12Zn, 20Bi, 4Mn	12	29	52	5.4 [c]
3, 26 µm	99.84	0.106	54	11	25	93	51Pb, 7Sb, 29P, 198Sn, 20Zn, 4Se	12	26	36	33.2
3, 49 µm	99.86	0.022	54	11	22	46	49Pb, 11Sb, 26P, 8Se, 810Sn, 12Zn, 1.6Bi,	37	49	70	12.2
4, (n/a) µm	n/a	1.130	n/a	n/a	n/a	n/a	n/a	n/a	n/a	n/a	Failed
5, 31 µm	n/a	0.211	n/a	n/a	n/a	n/a	n/a	14	31	43	11.9
C10100[a]	99.99	0.005	25	15	10	10	4Pb, 4Sb, 3P, 3Se, 1Sn, 1Zn, 1Bi, 0.5Mn	n/a	n/a	n/a	n/a

[a] ASTM B152-09: min limit for Cu; max limit for all other elements.

[b] Only non-conforming values to C10100 listed for powders; max values for C10100.

[c] No flow through MPIF 3 standard funnel with 50 g of powder (i.e., method used for other measurements). Value obtained from flow of 100 g of powder through a 0.2 in. diameter funnel.

Table 2 – Spray conditions employed in various development stages.

	Powder Selection	General Coating Development		UFC Optimization and Prototyping
	N_2-spray	N_2-spray	He-spray	N_2 and He-spray
System	PCS-1000	PCS-1000	Kinetiks 4000	PCS-800, PCS-1000
Powder, d_{50} (μm)	20, 23, 26, 29, 42, 49	23, 42	42	42
Gas temp., T_g (°C)	400, 600, 800	400, 500, 600, 700, 800	350	600, 800
Gas pressure, P_g (MPa)	2, 3, 4	3, 5	3.5	5
Traverse speed (mm/s)	300	60, 100, 1000	100	Various
Step size (mm)	1	1	1.25	Various
Standoff distance (mm)	25	25, 100, 200	40	30

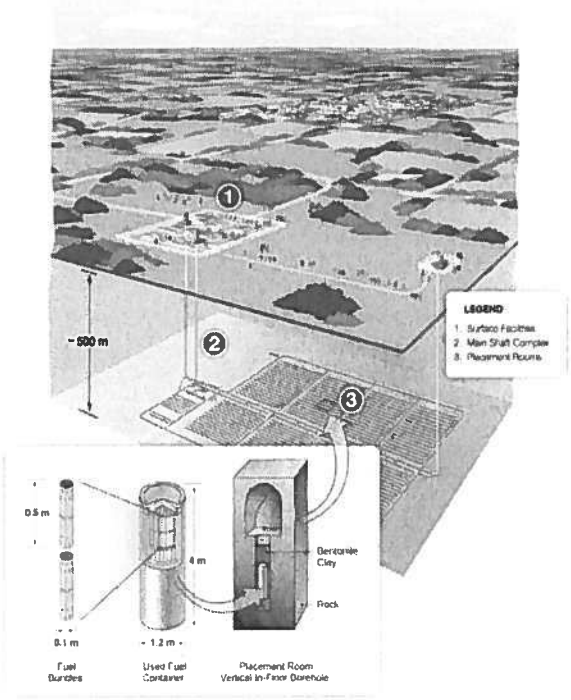

Figure 1 – Deep geological repository concept.

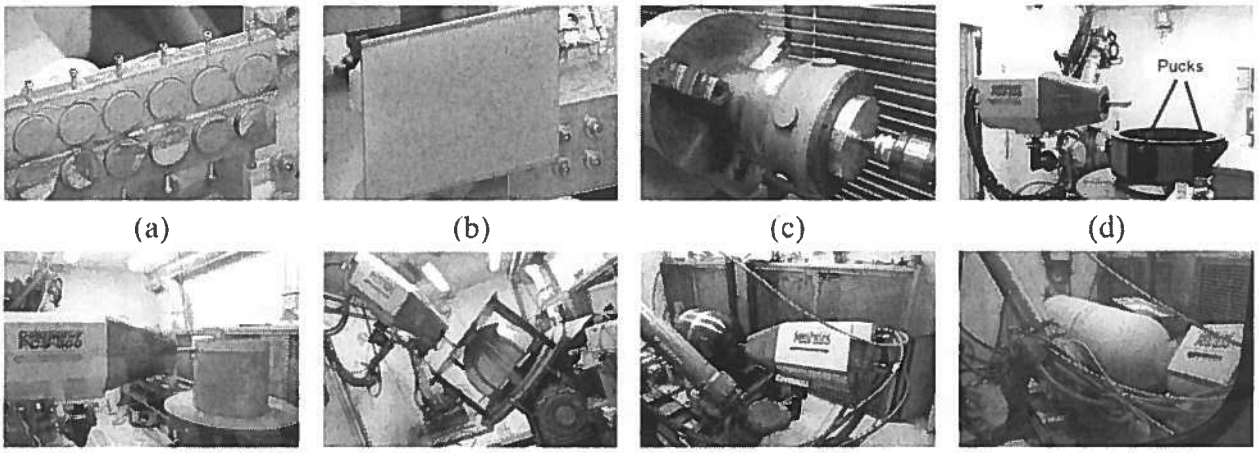

Figure 2 – Coating setups for (a-b) general coating development, (c-d) UFC coating optimization, and (e-h) prototyping.

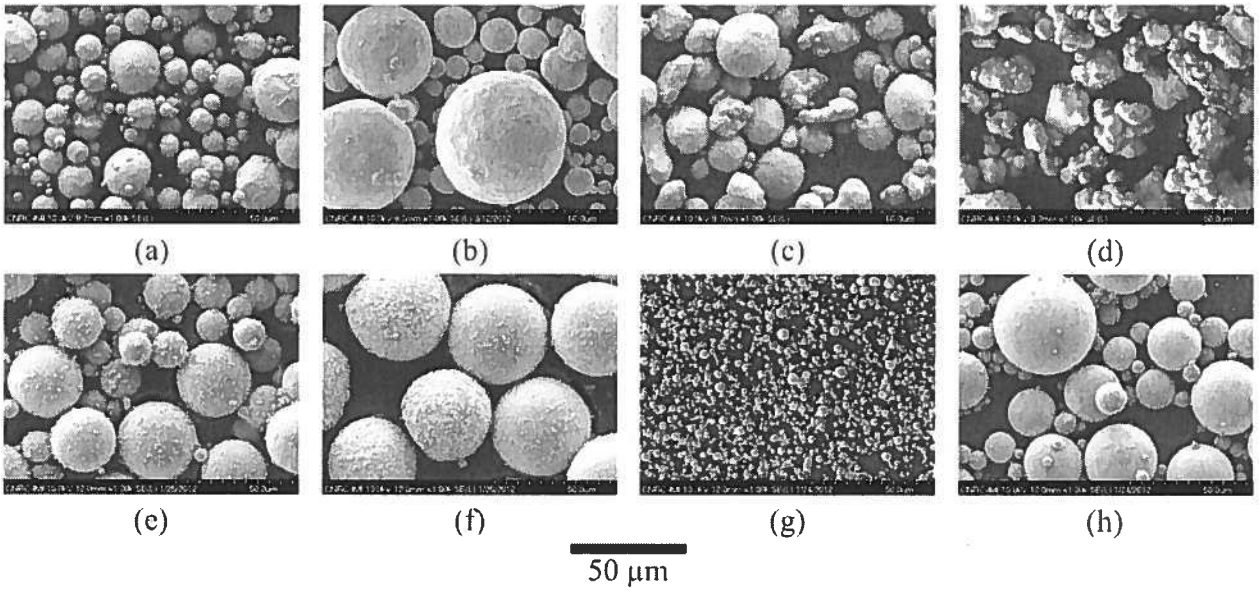

Figure 3 – Feedstock powder morphologies: (a) supplier 1, d_{50} = 20 µm; (b) supplier 1, d_{50} = 42 µm; (c) supplier 2, d_{50} = 23 µm; (d) supplier 2, d_{50} = 29 µm; (e) supplier 3, d_{50} = 26 µm; (f) supplier 3, d_{50} = 49 µm; (g) supplier 4, d_{50} = n/a; and (h) supplier 5, d_{50} = 30 µm.

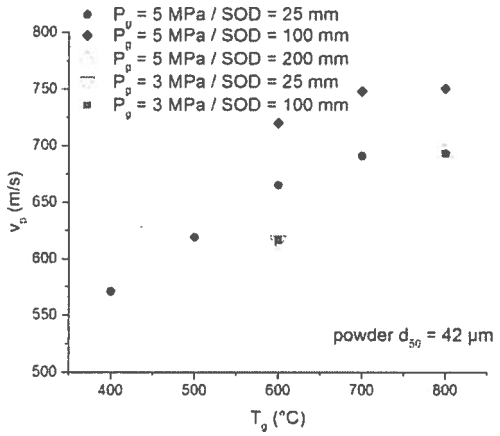

Figure 4 – Particle velocity for d_{50} = 42 µm powder versus gas temperature at various gas pressures and standoff distances.

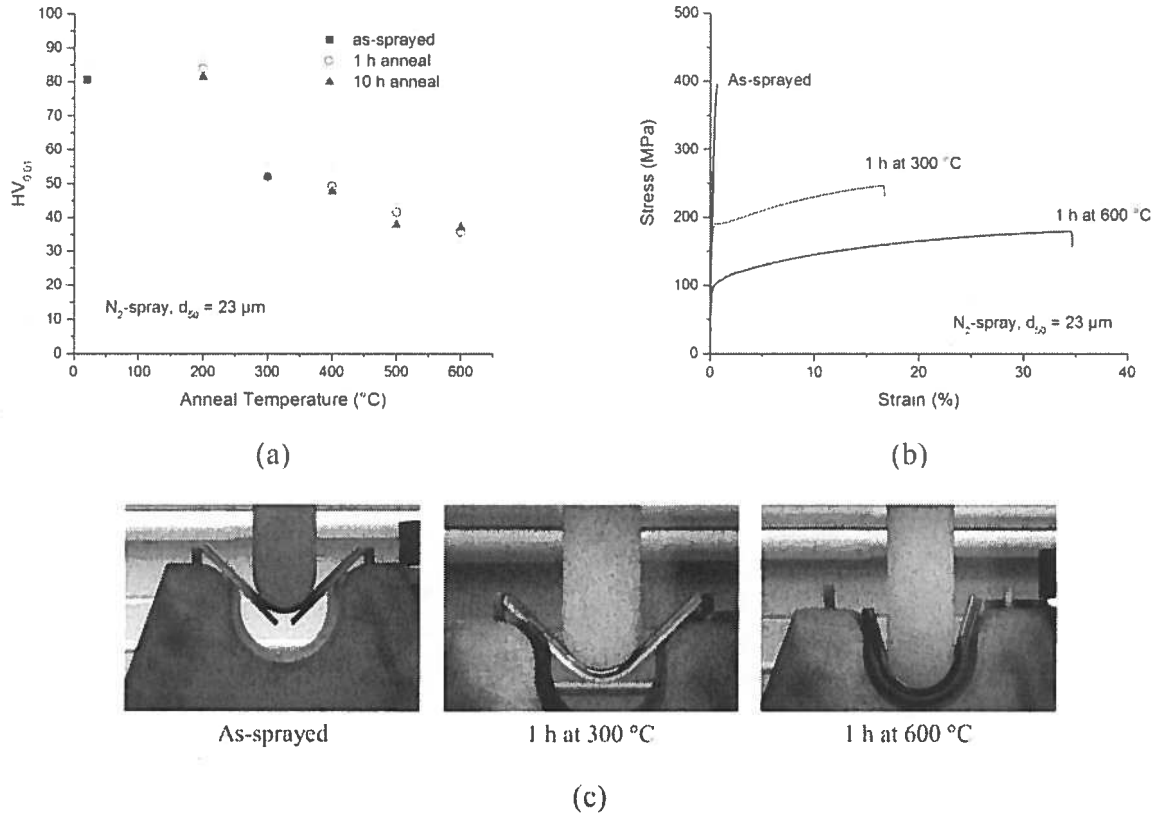

Figure 5 – Selected mechanical test results for N_2-sprayed coatings (d_{50} = 23 µm powder) after annealing at various temperatures: (a) microhardness as a function of anneal temperature, (b) stresss strain curves, and (c) photos of bend test specimens.

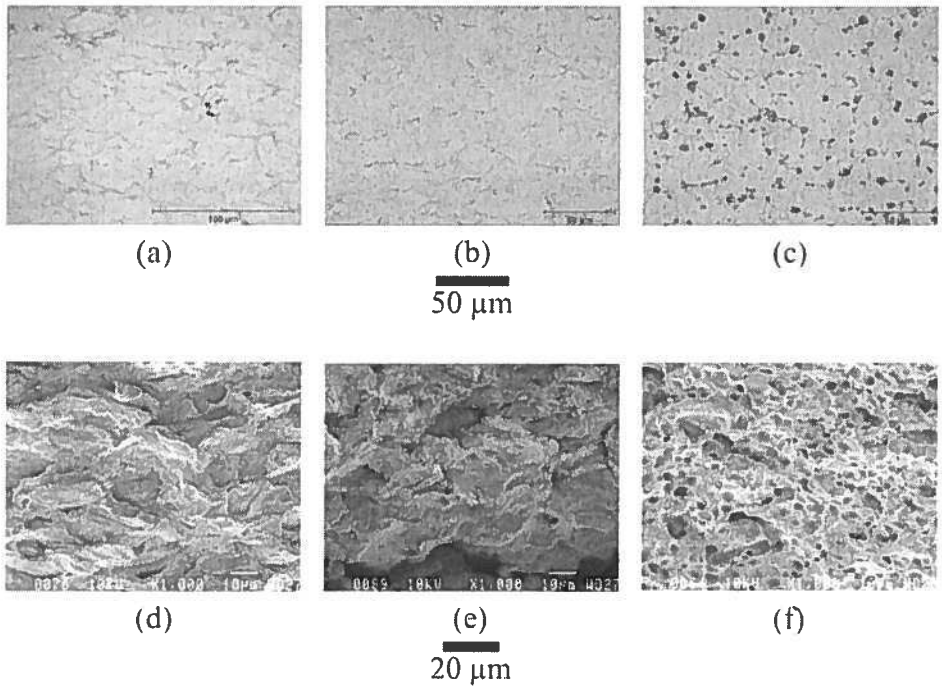

Figure 6 – Selected metallographic results for N_2-sprayed coatings (d_{50} = 23 µm powder) after annealing at various temperatures: etched microstructures obtained (a) as-sprayed, (b) after 300 °C/1 h anneal, and (c) after 600 °C/1 h anneal; and fracture surfaces of tensile specimens (d) as-sprayed, (e) after 300 °C/1 h anneal, and (f) after 600 °C/1 h anneal.

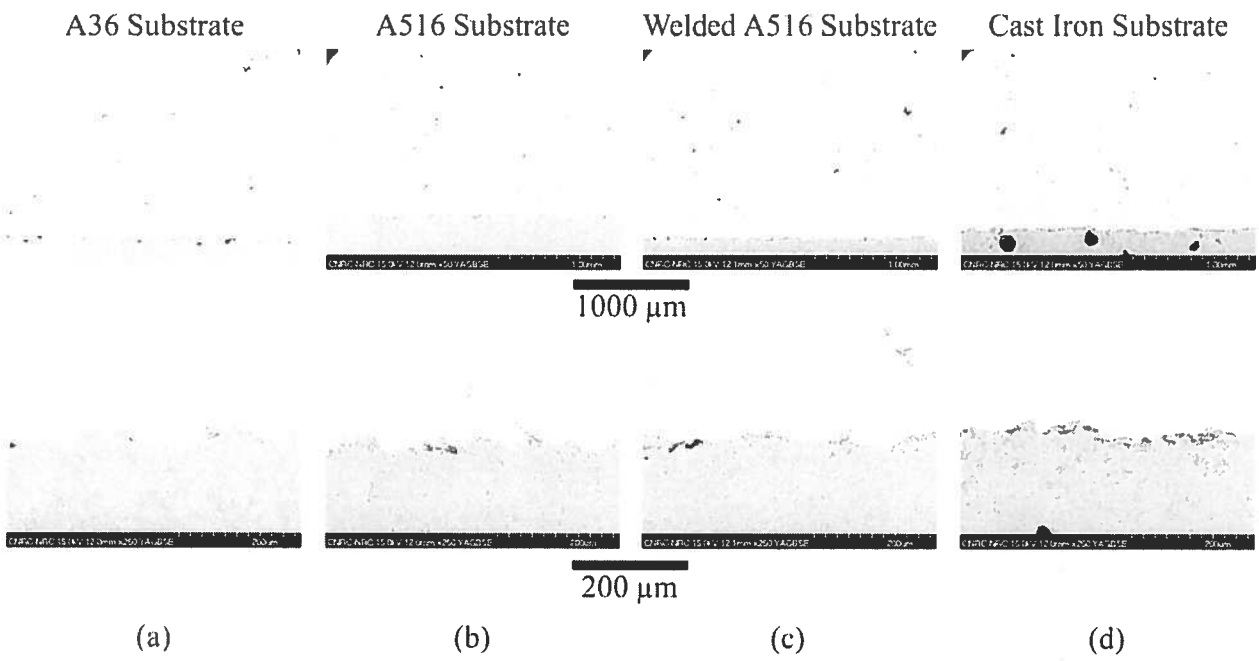

Figure 7 – Selected results for N_2-sprayed coatings (d_{50} = 42 µm powder) produced during UFC optimization: as-polished coatings sprayed using: initial reference parameters with T_g = 800 °C on (a) A36 substrate; and optimized reference parameters with T_g = 600 °C on (b) A516 grade 70 substrate, (c) welded A516 grade 70 substrate, and (d) cast iron substrate.

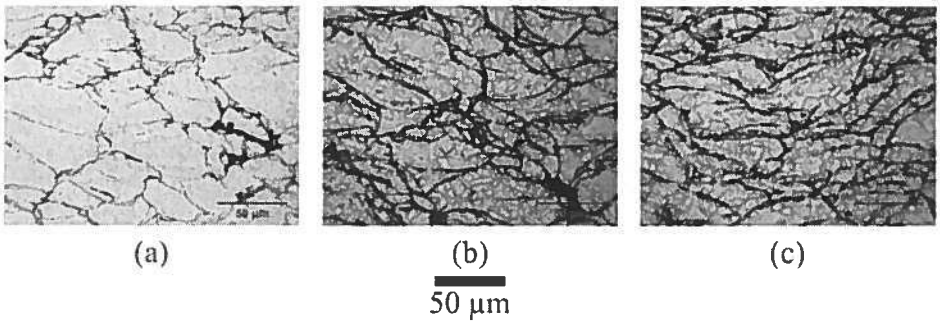

Figure 8 – Etched microstructures for N_2-sprayed coatings (d_{50} = 42 µm powder): (a) as-sprayed, (b) after 350 °C/1 h anneal, and (c) after 400 °C/1 h anneal.

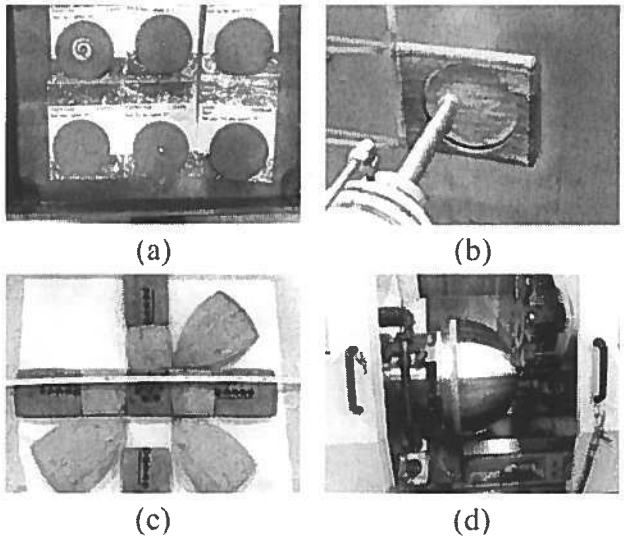

Figure 9 – Photos showing coating development for hemispherical head: (a) coated dishes (with matching geometry to the apex) used in the optimization of a curved spray pattern, (b) apex coated using an XY pattern with masking, (c) coated hemisphere sectioned for characterization, and (d) CNC machining of a coated hemisphere.

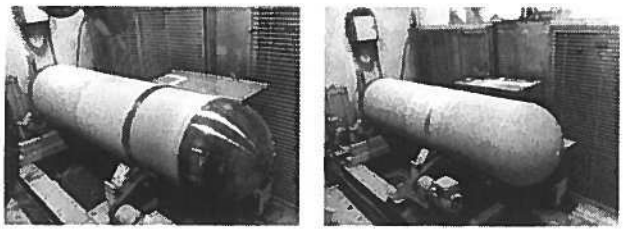

(a) (b)

Figure 10 – Full sized lower assembly after coating of (a) two sections and (b) entire assembly.